Positioning Device for Outdoor Mobile Robots Using Optical Sensors and Lasers

ISAKU NAGAI [a,*], GENKI YAMAUCHI [b], KEIJI NAGATANI [b], KEIGO WATANABE [a] and KAZUYA YOSHIDA [b]

[a] *Department of Intelligent Mechanical Systems, Okayama University, 3-1-1 Tsushima-naka, Kita-ku, Okayama, 700-8530, Japan*

[b] *Graduate School of Engineering, Tohoku University, 6-6-01, Aramaki-Aoba, Aoba-ku, Sendai, 980-8579, Japan*

[*] *e-mail: in@sys.okayama-u.ac.jp*

Abstract

We propose a novel method for positioning a mobile robot in an outdoor environment using lasers and optical sensors. Position estimation via a noncontact optical method is useful because the information from the wheel odometer and the global positioning system in a mobile robot is unreliable in some situations. Contact optical sensors such as a computer mouse are designed to be in contact with a surface and do not function well in conditions with strong ambient light. To mitigate the challenges of an outdoor environment, we developed an optical device with a bandpass filter and a pipe to restrict solar light and detect translation. The use of two devices enables sensing of the mobile robot's position, including posture. Furthermore, employing a collimated laser beam allows measurements against a surface to be invariable with the distance to the surface. In this paper, we describe motion estimation, device configurations, and several tests for performance evaluation. We also present the experimental positioning results from a vehicle equipped with our optical device on an outdoor path. Finally, we discuss an improvement in postural accuracy by combining an optical device with precise gyroscopes.

Keywords: Mobile robot, Position estimation, Laser speckle pattern, Optical sensor

1. INTRODUCTION

Information on position and orientation is a fundamental requirement for controlling a mobile robot running on a planar ground. Many methods and sensing systems that recognize a robot's position have been presented previously. However, information gathered by a global positioning system is often inaccurate owing to multipath error [1], and its output rate is comparatively slower than other sensors.

An odometer with wheel encoders is commonly used; however, it is quite unreliable because of wheel slippage and vehicle skidding. On the other hand, optical sensors designed for optical mice or laser mice are available for measuring the robot position since they detect motion from the ground movement without encoders' information. Therefore, the positioning device using the optical sensor has advantages in application to mobile robots or vehicles [2]. Advantages of using an optical sensor include the following: low cost, compact, high speed, kinematics-free, and noncontact sensing. Applications of using a mouse sensor for positioning or navigation of a mobile robot have been studied and are outlined as follows. A combination of an optical mouse with a compass allows the evaluation of a robot's position [3]. A single optical sensor also enables measurement of a robot's position, including rotation [4]. The use of two mouse sensors enables a mecanum-wheeled mobile robot, which has omnidirectional locomotion and is controlled to precisely move along an intended path [5]. Nonsystematic errors from the odometer using a pair of optical mice can be reduced via redundant measurements [6]; multiple optical sensors provide a more accurate estimation of the position and posture [7, 8, 9]. The resolution of each optical sensor is usually calibrated by certain methods for correcting the measurement accuracy [10, 11]. However, the distance between the optical sensor and the ground surface must be small for those methods. Unfortunately, these sensors are not suitable when applied to the positioning of an outdoor mobile robot because the variation in the sensor/ground distance negatively affects the accuracy of the measurement. To mitigate this, a standard focal length lens is used, where height measurements are acquired to convert the sensor output into actual travel information [12]. For larger heights from the ground, the combination of a sensor and a lens with a longer focal length is effective [13]. A telecentric lens enables the size of an object to appear constant; however, the maximum velocity of motion estimation is consequently restricted by its narrow area of view. Moreover, the telecentric lens occupies a large space in a robot compared to standard lenses [14]. Another solution is combining an optical sensor with a laser instead of a lens for motion measurements with a larger distance between the sensor and the ground surface [15]. This method uses images of a speckle pattern produced by the laser light source for the tracking in the sensor. Despite the absence of a lens, the measurement error of the translation is small for different heights, owing to the characteristics of the speckle pattern. However, the laser spot on the surface disappears if the device is in an outdoor environment. Therefore, the sensor does not output any position information in a strong ambient light condition. The optical sensors also have a characteristic of accumulative error like inertial sensors, but even more reliable and robust position measurement can be achieved by combining newly developed optical sensors with conventional sensors for local positioning and global positioning device.

Our objective is to develop a noncontact positioning system that estimates the position of a mobile robot; the noncontact positioning system should be impervious to the height of the sensor and to solar light in an outdoor environment. A robust estimation using redundant optical sensors has been achieved, in spite of obstructions and height variations [16]. However, the performance in outdoor

conditions was not investigated in the research. We propose a device combining an optical sensor with a bandpass filter to practically reduce solar light. Additionally, a well-collimated laser beam is used for precisely estimating the translations of the device on a surface for different heights. We demonstrate the maximum velocity supported by the device after an explanation of the characteristics of the laser speckle pattern and the manufactured device configuration. Our compact device is easily mounted on a mobile robot for independent positioning from the kinematics of the robot. The experimental data of the tracking of a vehicle equipped with this positioning device running in outdoor environment is given. Finally, we show the results of an experiment that improved the postural accuracy by fusing the translation of an optical device with the information of inertial sensors, including gyroscopes.

2. MOTION ESTIMATION USING OPTICAL SENSORS

2.1. Characteristics of laser speckle patterns

Optical mice sensing technology that measures displacement on a surface is categorized into two groups. The first group involves optical mice, in which the pattern of a surface material is photographed by an image sensor with illumination by a red or blue LED. The planar motion is determined by gauging the horizontal and vertical shifts between two adjoining images. The other group involves laser mice, in which a laser speckle pattern from a laser beam being projected onto an object is photographed by an image sensor. Motion is estimated through the tracking of images in the sensor, in a manner similar to the estimation of motion of optical mice. The laser speckle is a random and high-contrast pattern caused by the interference of laser rays reflecting from an object's surface, and it is observed even without lenses in spaces where the spot of the laser is seen. The displacement of the speckle pattern observed when an object surface is translated or rotated is detailed in the literature by Yamaguchi [17], where we focused on the theory of the speckle displacement. If an object surface is not strained, the displacement of the speckle pattern detected on an image sensor by using a collimated laser beam is simplified as

$$A_x = a_X \cos\theta_O - a_Z \sin\theta_O - L_O\left[-\Omega_Y\left(\frac{\cos\theta_S}{\cos\theta_O} + 1\right)\right]$$
$$A_y = a_Y - L_O[-\Omega_X(\cos\theta_S + \cos\theta_O) - \Omega_Z(\sin\theta_S + \sin\theta_O)] \quad (1)$$

where the vector (A_x, A_y) is the speckle displacement in an observation plane, as shown in Figure 1. (a_X, a_Y, a_Z) and (Ω_X, Ω_Y, Ω_Z) are the translation and rotation of the illuminated object region, respectively. L_O and θ_O are the distance and direction to the observation plane, respectively. Furthermore, θ_S is the incident angle of the laser beam. If we adopt a collimated beam, the speckle

displacement is independent of L_S [17], which is the distance to the laser source.

We assume that the mobile robot runs along a flat ground, and that the laser beam is perpendicularly pointed at the ground plane. Therefore, the angle $\theta_S = 0$, the rotation $\Omega_X = 0$, the rotation $\Omega_Y = 0$, and the translation $a_Z = 0$. Using these assumptions, the displacement is represented as

$$A_x = a_X \cos\theta_O$$
$$A_y = a_Y + \Omega_Z L_O \sin\theta_O. \tag{2}$$

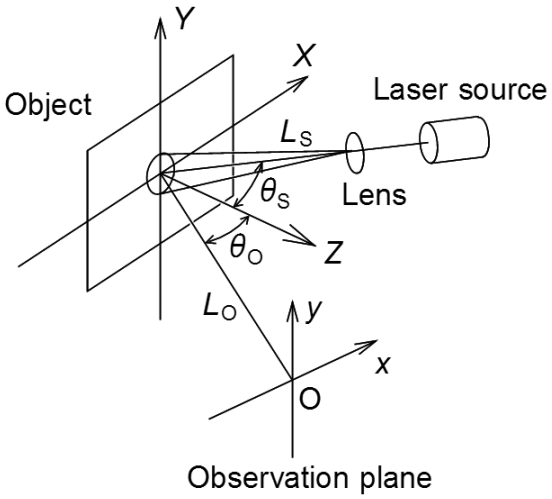

Figure 1: Optical system for detecting two-dimensional speckle displacement.

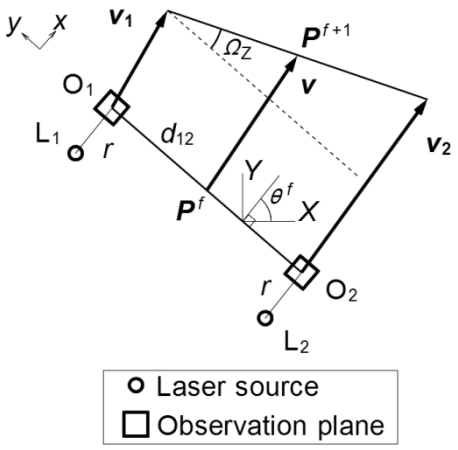

Figure 2: Translation and rotation determined from displacement at two observation points.

2.2. Sensor layout and motion estimation

Two optical sensors and their accompanying laser sources are positioned a distance d_{12} apart at O_1 and O_2 to obtain the translation vector $\boldsymbol{v}$ and the rotation Ω_Z of the positioning device, as shown in Figure 2. In the figure, r is the distance from the origin of the observation plane to the laser source, which is equal to $L_O \sin\theta_O$ in Eq. (2). In Figure 2, $\boldsymbol{v}_1 = [a_{X1} \quad a_{Y1}]^T$ and $\boldsymbol{v}_2 = [a_{X2} \quad a_{Y2}]^T$ are the translations of the points O_1 and O_2, respectively. We define the robot position as $\boldsymbol{P}$, which is the center of the segment O_1O_2. We also define h as the height of the observation plane from the object surface.

In Eq. (2), $\cos\theta_O$ indicates a decrease of the speckle displacement A_x caused by the incident angle θ_O of the observation plane in the original optical system, as shown in Figure 1. However, the sensor plane in our positioning device is not inclined toward the object surface. Both of the displacements A_x and A_y that output from an optical sensor are the same when the sensor is translated along the x- or y- axis. Therefore, $\cos\theta_O$ in the equation is supposed to be 1.

From Eq. (2) and the assumptions above, the displacement vectors $[x_1 \; y_1]^T$ and $[x_2 \; y_2]^T$ on the observation planes O_1 and O_2 are

$$\begin{bmatrix} x_1 \\ y_1 \end{bmatrix} = \boldsymbol{v}_1 + \begin{bmatrix} 0 \\ r\Omega_Z \end{bmatrix} = \begin{bmatrix} a_{X1} \\ a_{Y1} + r\Omega_Z \end{bmatrix} \tag{3}$$

$$\begin{bmatrix} x_2 \\ y_2 \end{bmatrix} = \boldsymbol{v}_2 + \begin{bmatrix} 0 \\ r\Omega_Z \end{bmatrix} = \begin{bmatrix} a_{X2} \\ a_{Y2} + r\Omega_Z \end{bmatrix} \sim \begin{bmatrix} a_{X1} + d_{12}\Omega_Z \\ a_{Y2} + r\Omega_Z \end{bmatrix} \tag{4}$$

From Eqs. (3) and (4), the rotation Ω_Z and translation $\boldsymbol{v}$ are estimated as in Eq. (5).

$$\begin{aligned} \Omega_Z &= \frac{x_2 - x_1}{d_{12}} \\ \boldsymbol{v} &= \frac{1}{2}(\boldsymbol{v}_1 + \boldsymbol{v}_2) = \begin{bmatrix} (x_1 + x_2)/2 \\ (y_1 + y_1)/2 - r\Omega_Z \end{bmatrix} \end{aligned} \tag{5}$$

The current position and posture of a mobile robot are determined by accumulating the translation vector and rotation at every frame as in Eq. (6).

$$\boldsymbol{P}^{f+1} = \boldsymbol{P}^f + \mathbf{Rot}(\theta^f)\boldsymbol{v} \tag{6}$$

$$\theta^{f+1} = \theta^{f} + \Omega_{Z},$$

where **Rot**() is a two-dimensional rotation matrix, and f is the number of time-series data.

2.3. Device configuration

The Avago ADNS-6010 [18], designed for a laser mouse, is employed as the optical sensor in our positioning device, but the original lens and infrared laser source are not used. We combine the sensor with a substitutive 650 nm laser. Additionally, we make a 4 mm aperture by drilling the original small hole in front of the cover of the sensor. From these modifications, the sensor receives the reflected laser rays from an object surface at a distance much larger than that of a normal mouse. An optical sensor has an image sensor of a 30× 30 pixel resolution that detects the speckle displacement by calculating the correlations between the images. The shutter period and frame rate in the sensor are automatically changed for capturing images with optimum brightness and contrast. Therefore, the frame rate varies from 1000 to 5000 fps. The sensor internally accumulates the speckle displacement at every captured frame to produce the position and posture of the mobile robot. Therefore a microcomputer can read all the displacements even at a lower speed than the frame rate of the sensor. In our device, a SH2/7125 microcomputer executes this reading at a rate of 1667 Hz, and provides the positions of two optical devices by accumulating the speckle displacement. A PC in a mobile robot retrieves the accumulated translations of two optical devices at a rate of approximately 90 Hz and derives relative translations by subtracting the former position from the current position before estimating the position and rotation. By using a resolution value of the optical sensor of 0.0838 mm/count, the PC converts the units from counts to mm. The microcomputer is connected to the PC by a USB interface for the power supply (5.0 V/0.3 A) and communicates at a baud rate of 390 kbps using a USB-serial adapter.

The optical sensor board and microcomputer board we manufactured are shown in Figure 3. The distances between the optical sensor and the laser source and between the optical sensor and object surface are shown in Figure 4, where h is distance between the optical sensor and the object surface. The r, mentioned above is 16 mm, as shown in Figure 4.

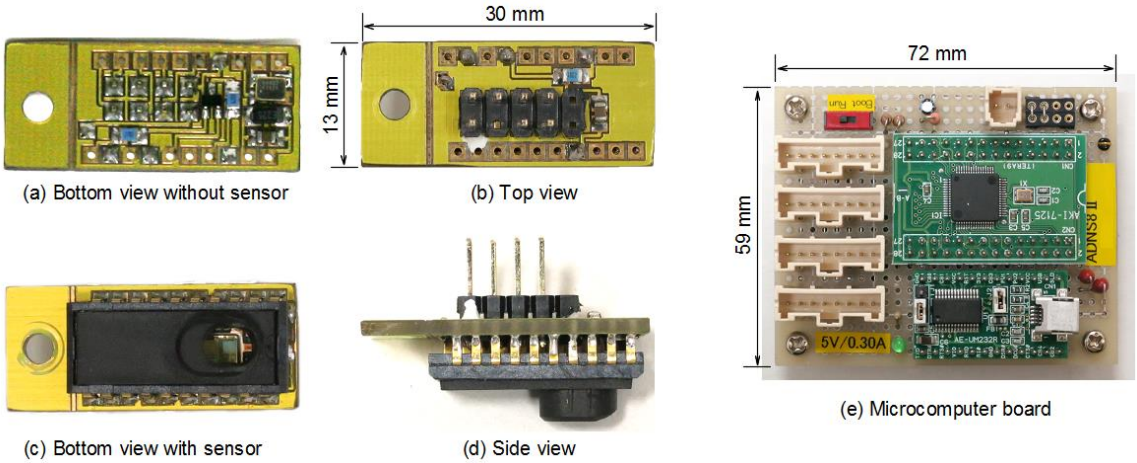

Figure 3: Optical sensor board (a)-(d) and microcomputer board (e).

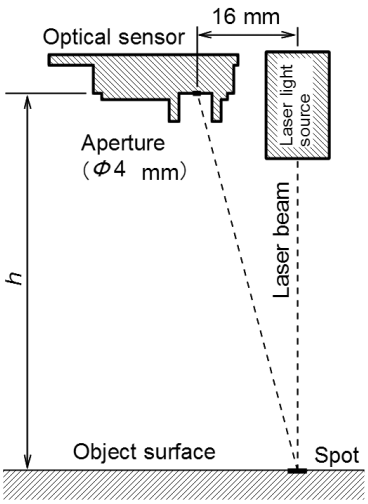

Figure 4: Distances between the object surface and the optical sensor and between the optical sensor and laser source.

3. PERFORMANCE TESTS

3.1. Height invariability

We tested our device to determine the error in position with respect to the height *h*. The positional accuracy was evaluated by comparing positions estimated by the device with the translation commands to a robot arm (Mitsubishi RV-M2). The device was fixed to the end of the wrist joint and then moved on paper, as shown in Figure 5. The robot arm has a precision of 0.1 mm for the position and 0.1° for the rotation. The device was moved 100 mm in a direction on the paper at a velocity of 0.05 m/s at a specified height *h* above white and black paper. The error of the estimated position for different heights is shown in Figure 6. The error suddenly escalated at certain heights because the laser spot became invisible to the sensor or because the speckle pattern disappeared at a large *h*. In the

ambient light condition of 700 lx, which is normal illuminance in a room, the sensor covers a wider height range on white paper because it induces a stronger reflection of the laser spot than the black paper does. If the sensor is used in a darker condition, such as 100 lx, the available height range of black paper increases as much as that of the white paper. The results also show that the measurement error remained under 1.6% at heights between 50 mm and 140 mm. The capability of being used over a wide height range enables the device to be adapted easily to different robots.

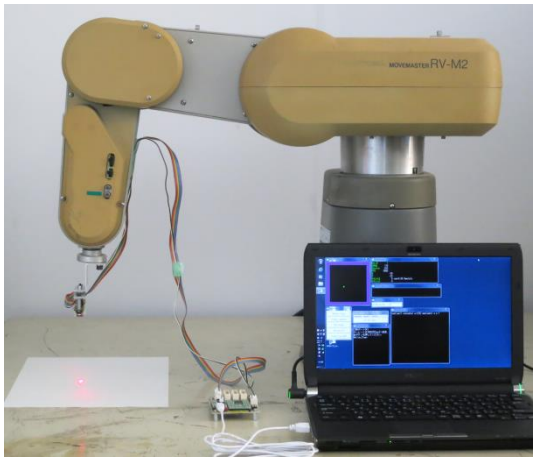

Figure 5: Robot arm for moving optical device at a specified height.

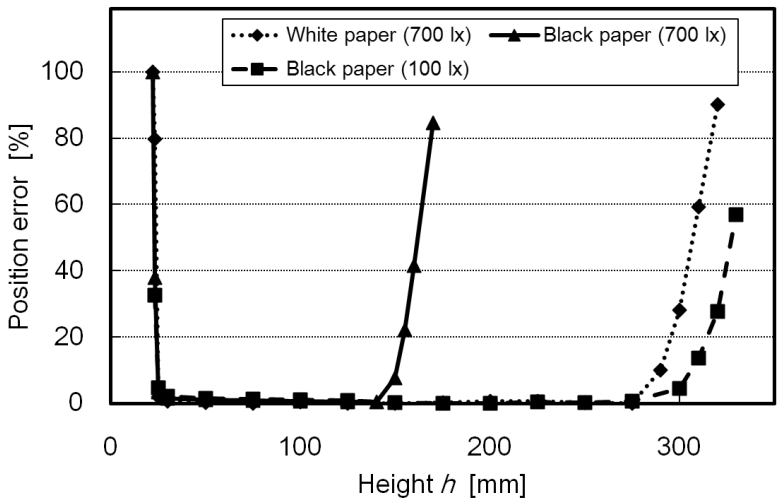

Figure 6: Position error for different heights.

3.2. Maximum velocity supported

We investigated the maximum velocity supported by the position measurement device. The optical device was fixed to a linear stage, and the paper attached to a plastic plate was turned by an actuated

turntable, as shown in Figure 7. The rotational speed of the turntable was measured by a noncontact optical tachometer (testo 465). The actual velocity of the surface is calculated using both the rotation rate and the radius of the sensor position. As shown in Figure 8, the maximum velocity that the sensing device can measure was 2.3 m/s on a white paper and 1.8 m/s on a black paper. These maximum velocities are sufficient for conventional outdoor mobile robots. The ideal line in Figure 8 shows velocity when the measured value has no errors. The estimated velocity is approximately 3% lower than the actual velocity in the experiment, which affects position estimation.

Another test was carried out to investigate the relationship among the maximum velocity, shutter period, and frame rate of the optical device. The shutter period and frame rate automatically vary to maintain a level of brightness of the image in the sensor. White and black paper was used, and the height *h* was increased so that the sensor operated at a longer shutter period and a lower frame rate for the test. Figure 9 shows that the maximum velocity is related to both the shutter period and the frame rate. The velocity measurements of the robot equipped with this positioning device are strongly restricted by the shutter period; therefore, the laser spot or the ambient light must be at a certain level of illuminance for the device to measure properly.

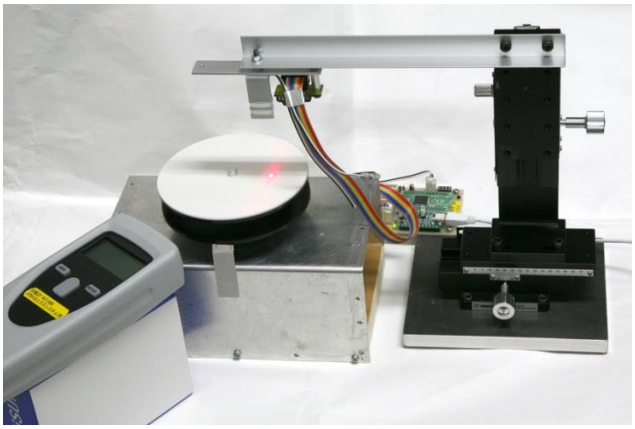

Figure 7: Turntable driven by motor for measuring maximum velocity of tracking.

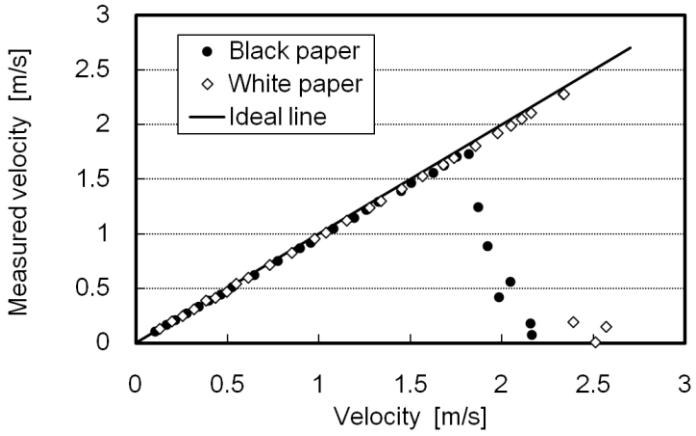

Figure 8: Maximum velocity supported by an optical sensor.

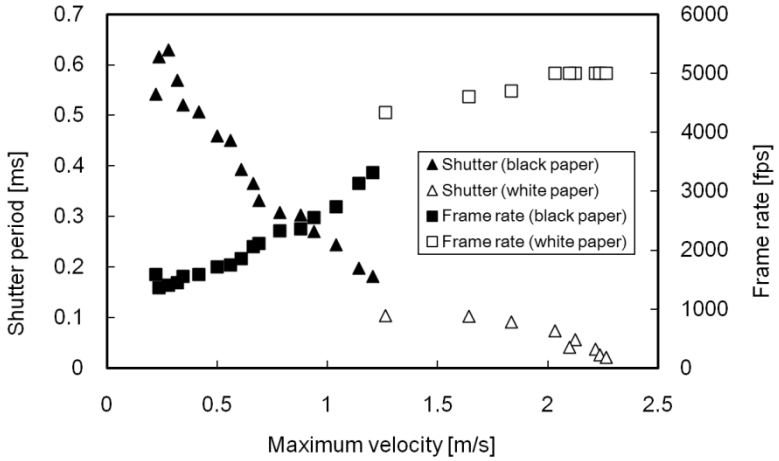

Figure 9: Relationship among maximum velocity, shutter period, and frame rate.

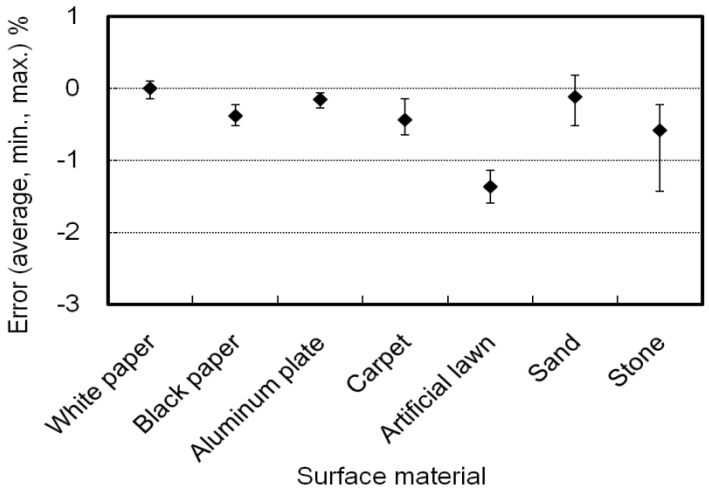

Figure 10: Position error for different surface materials.

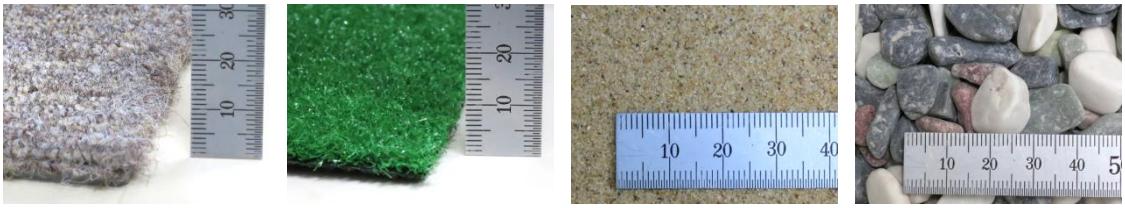

(a) Carpet (b) Artificial lawn (c) Sand (d) Stone

Figure 11: Surface materials used for investigating measurement capability.

3.3. Different surface materials

We also investigated the measurement capability for different surface materials. Figure 10 shows the relative error of the position estimated by the device after it traveled 200 mm in a direction at a velocity of 0.05 m/s and a height of 100 mm. Figure 11 shows some of the surface materials used for the test. The device was moved 10 times for each material. The artificial lawn greatly reduced the illuminance of the laser spot because of the green coloring, resulting in the sensor struggling with tracking. The device estimated motions well on bright surfaces, such as white paper and aluminum plates. The error of the device was between –1.6% and 0.2% from different surfaces used in the test.

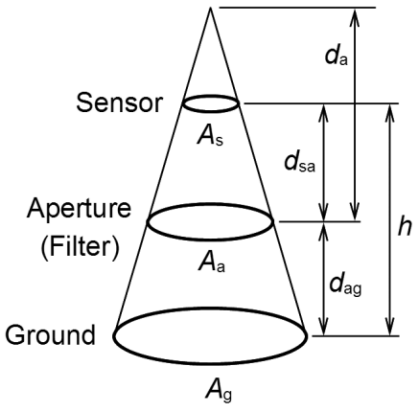

Figure 12: Aperture model of visible ground area.

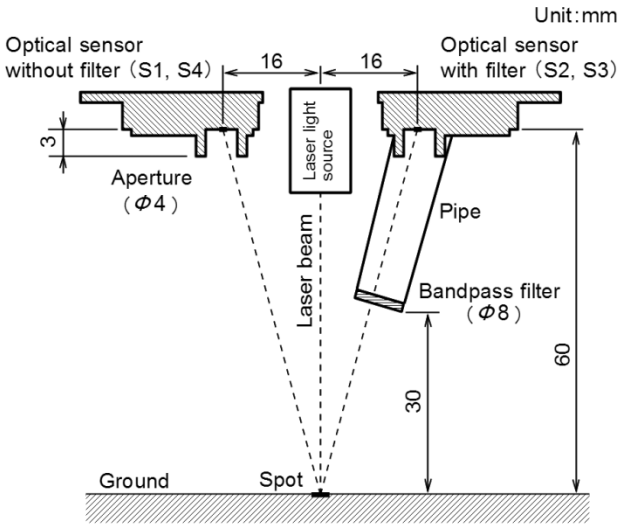

Figure 13: Distances between the ground and optical sensor, laser light source, and bandpass filter.

4. POSITION ESTIMATION OF A VEHICLE

4.1. Restricting solar light

4.1.1. Theory

An optical device detects a robot's translation by processing images of the speckle pattern produced by laser light. However, the device also receives ambient light, which is much stronger when it is in an outdoor environment, and thus an optical device does not function in that condition at all. Therefore, it is necessary for a device in an outdoor environment to restrict solar light. We propose a method for reducing the solar light, which is strong.

First, we estimate a ratio of radiant illumination between the laser source and the solar light, where we consider the radiant illumination entering the image sensor. Applying an aperture model to the optical device defines A_{s}, A_{a}, and A_{g} as areas of the image sensor, the aperture, and the region on the ground that is visible from the sensor through the aperture, respectively, as shown in Figure 12. The distance between the image sensor and the aperture is d_{sa}, and the distance between the aperture and the ground is d_{ag}. d_{a} is the distance between the aperture and the vertex of the cone, which has sectional areas A_{s}, A_{a}, and A_{g}. The distance h between the image sensor and the ground equals $d_{\mathrm{sa}} + d_{\mathrm{ag}}$. A_{g} is represented by Eq. (7).

$$A_{\mathrm{g}} = \frac{\left(d_{\mathrm{a}} + d_{\mathrm{ag}}\right)^2}{{d_{\mathrm{a}}}^2} A_{\mathrm{a}} \tag{7}$$

$$= \frac{\left\{\left(1 - \sqrt{A_{\mathrm{s}}/A_{\mathrm{a}}}\right)^{-1} d_{\mathrm{sa}} + d_{\mathrm{ag}}\right\}^2}{\left(1 - \sqrt{A_{\mathrm{s}}/A_{\mathrm{a}}}\right)^{-2} {d_{\mathrm{sa}}}^2} A_{\mathrm{a}}$$

Eq. (7) shows that A_g can be estimated from A_s, A_a, d_{sa}, and d_{ag}. The optical device has an area of A_s = 1.61 mm^2 with a side length of 1.27 mm. A normal device, which does not restrict solar light, has an aperture of 4 mm at a distance of 3 mm below the sensor, which is 57 mm above the ground, as shown in Figure 13. From this, A_a= (4/2)$^2\pi$ = 12.6 mm^2, d_{sa} = 3 mm, and d_{ag} = 57 mm. Using these parameters, the region on ground is calculated to be A_g = 2.19 × 10^{-3} m^2 via Eq. (7). If the radiant illumination of mid-summer daylight is approximately 540 W/m^2, then the sensor receives a radiant power of $540A_g$ = 1181 mW of ambient light. In fact, the output power of a laser light source is only 3.42 mW; therefore, the ratio between the laser source and the solar light is 0.290%, which means the laser speckle pattern nearly disappears because of the solar light in the case of a normal device.

To assist the position measurement device in an outdoor environment, we modify it based on two schemes of restriction, that is, area and wavelength. For the area restriction, a pipe with a diameter of 8 mm and a length of 30 mm is attached in front of the image sensor toward the spot on ground, reducing A_g. By adding the pipe, both distances d_{sa} and d_{ag} become 30 mm and reduced area A'_g becomes 1.67 × 10^{-4} m^2, as calculated from Eq. (7) with parameters A_s = 1.61 mm^2, A_a= (8/2)$^2\pi$= 50.3 mm^2, $d_{sa} = 30$ mm, and $d_{ag} = 30$ mm. For the wavelength restriction, a bandpass filter that passes only a specified wavelength is inserted in the pipe, as shown in Figure 13. The specifications of the bandpass filter (Orion Optics O−BPF 650) used for the device are as follows: the center wavelength (CWL) is 650 nm, the full width at half maximum (FWHM) is 50 nm, and the transmittance is 90%. The filter blocks all ambient light, except light with a wavelength of approximately 650 nm. The reduction of the visible light for the sensor is approximately 11.1%, which is estimated by dividing the FWHM (50 nm) by the wavelength (850–400 nm). The radiant power in the modified device is reduced to 0.111 × $540A'_g$ = 10.0 mW. The ratio between the laser source and the solar light becomes 34.2%, which is much higher than the ratio of 0.290% for the normal device. These modifications enable the device to function in an outdoor environment.

4.1.2. Experiments of different illuminance values

We investigated the range of illuminance in which the optical device with the solar restriction was exposed to strong ambient light. We evaluated the device capability by surface quality (SQUAL), which is an output of the sensor. The SQUAL is defined by the manufacturer of the optical sensor, and indicates the number of valid features in a frame image captured by the sensor. The maximum SQUAL value is 169. Empirically, the sensor outputs approximately 130 SQUAL when the measurement conditions are good, and it does not output any signal when the SQUAL is less than approximately 30. We investigated the relationship between measurement error and SQUAL in advance, as shown in Figure 14. In the figure, SQUAL means the average of sensor output when it

was moved 200 mm at a velocity of 0.3 m/s on a white paper in different illuminance conditions. The graph shows the device adequately estimates translational motion in case that the SQUAL value is greater than 40.

The SQUAL values for different illuminance conditions are shown in Figure 15. A projector with an output power of 500 W was used to produce an illuminance of up to 70000 lx around the laser spot. The modified device with a pipe and a bandpass filter operated up to an illuminance of 70000 lx, while the normal device could not operate beyond 1600 lx. The difference of efficiency between the modified device and normal device is also seen in Figure 16, which shows SQUAL values and frame images captured by the optical sensor at different illuminance conditions. In the figure, the pattern-like salt-and-pepper noise in the images is the laser speckle pattern. It is confirmed that the SQUAL value was over 30 and high-contrast speckle was effectively observed in high illuminance conditions by the sensor S2 with the pipe and bandpass filter for restricting solar light. The ambient illuminance can also be up to 60000 lx in our experimental field, so the capability of the modified device for strong light is sufficient for our robot.

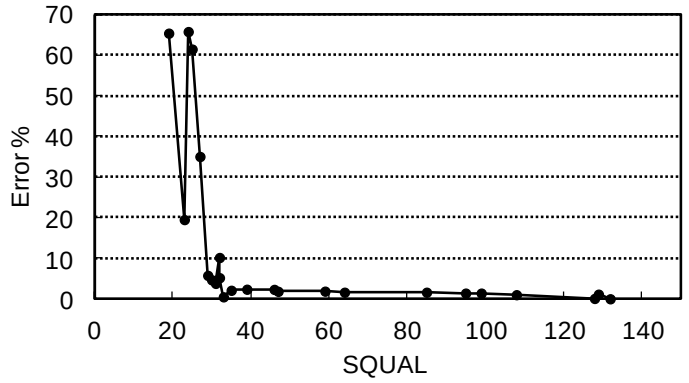

Figure 14: Measurement accuracy of optical sensor for different values of SQUAL.

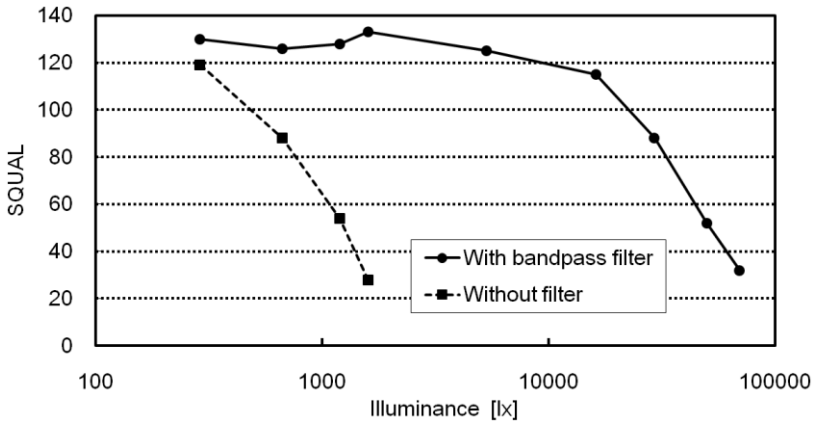

Figure 15: SQUAL values of optical sensor for different values of illuminance.

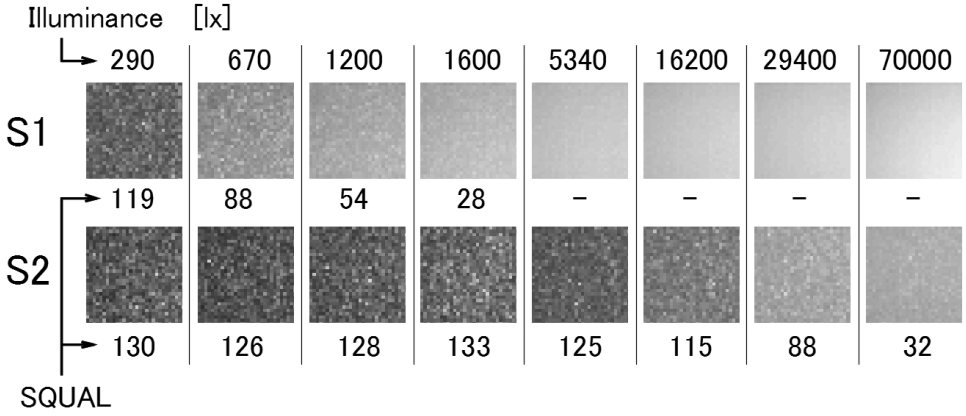

Figure 16: Frame images captured by optical sensors S1 and S2 for different values of illuminance.
(S1: Normal device, S2: Modified device with bandpass filter and pipe)

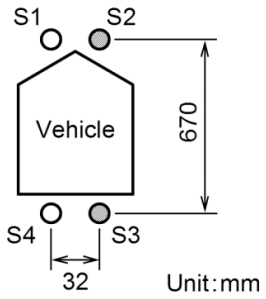

Figure 17: Layout of optical devices S1, S2, S3, and S4 in a vehicle.

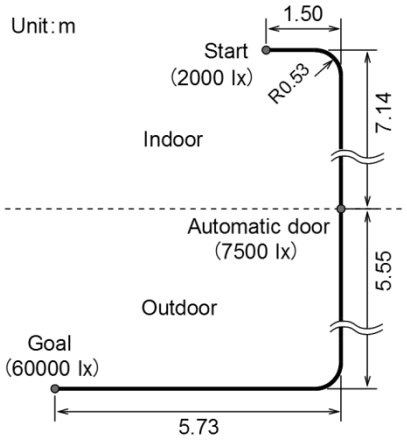

Figure 18: Length of course for experiment.

4.1.3. Positioning a vehicle in indoor and outdoor environment

The position measurement device that restricts solar light was evaluated with a vehicle moving in indoor and outdoor environments. The normal and modified devices were combined with a laser source, as shown in Figure 13, and attached to both the front and rear end of the vehicle, as shown in Figure 17. The heights of all sensors from the ground were approximately 70 mm. The sensors S1 and S4 comprise the normal device, and the sensors S2 and S3 comprise the modified device. One trajectory was estimated by the sensor pair S1 and S4, and the other trajectory was estimated by S2 and S3. A vehicle with four steering and driving wheels was manually moved three times in a sunny day at a velocity of 0.3 m/s from a start point to a goal point along the joint line of tiles on the ground, shown in Figure 18. The vehicle began at the start point in a building, passed through an automatic door, and reached the goal outside the building. The illuminance values at the start, at the automatic door, and at the goal are 2000 lx, 7500 lx, and 60000 lx, respectively. Figure 19 shows the vehicle moving in front of the automatic door near the goal point and the optical devices attached to the front of the vehicle.

Figure 20 shows the estimated trajectories using the normal and modified devices. In the figure, the trajectories from three trials are overlapped in each graph. The trajectories broke away from the intended path before passing the automated door in Figure 20(a), which was estimated by the device without filters and pipes; this happened because the solar light entered through the transparent automatic door. The trajectories estimated by the modified device continued to the goal point in spite of posture errors, as shown in Figure 20(b). The postural errors are due to translational errors that each optical sensor has. The restriction of solar light by a bandpass filter and a pipe enables the use of the sensor in an outdoor environment.

The effect of the bandpass filter and the pipe can be observed in the SQUAL value output from the optical device. Figure 21 shows the SQUAL record as the vehicle moved from the start point to the goal point. S1 indicates the normal device, and S2 indicates the modified device. The horizontal axis of the graph is time, and the automatic door passing is at 22.8 s. The SQUAL of S1 stopped updating before passing the door, except for the moment at the rail of the door. The most of the SQUAL values of S2 remained above 30, which means the modified device estimated the motion precisely in the outdoor environment.

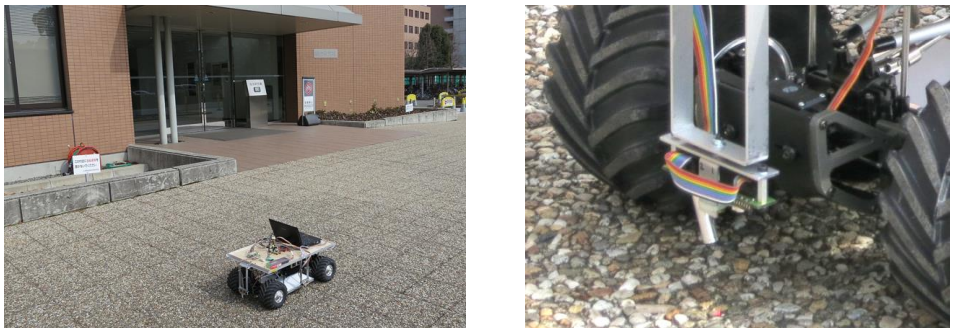

(a) Vehicle running near outdoor goal (b) Optical device in front of vehicle

Figure 19: Vehicle for experiment.

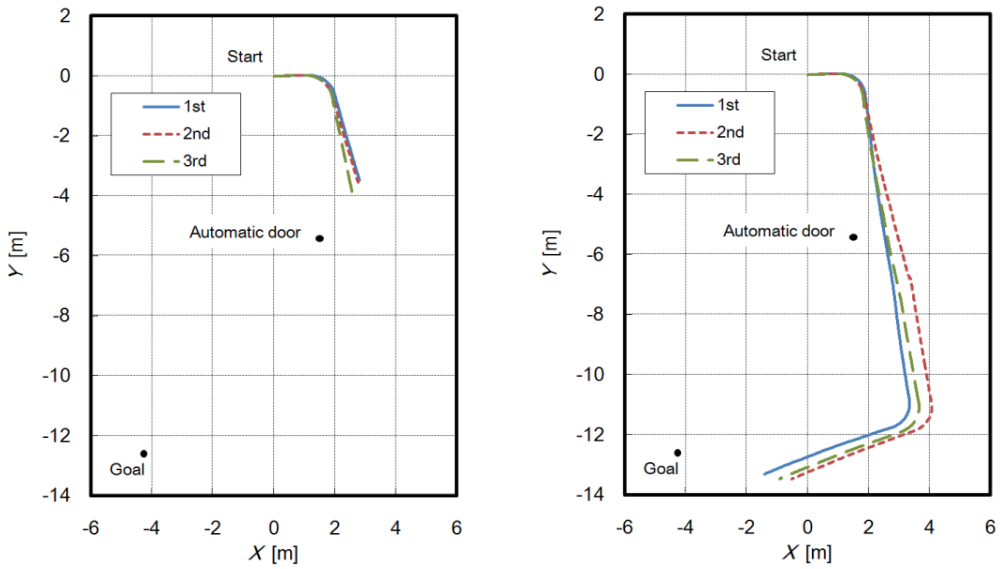

(a) Trajectory estimated by normal device (b) Trajectory estimated by modified device using bandpass filter and pipe

Figure 20: Estimated trajectory of vehicle.

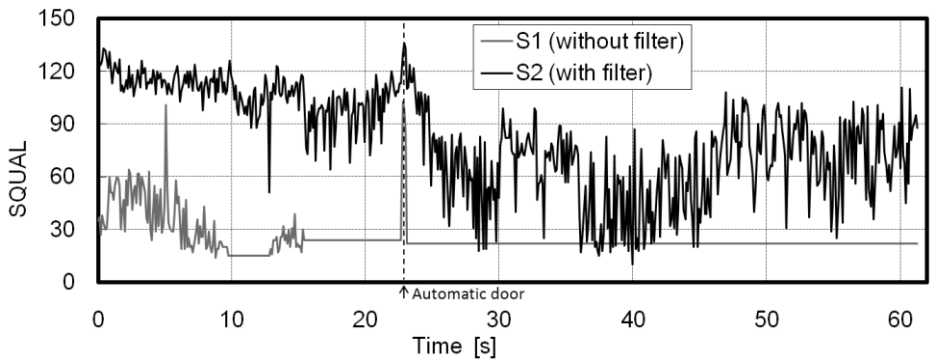

Figure 21: Record of SQUAL values from start to goal.

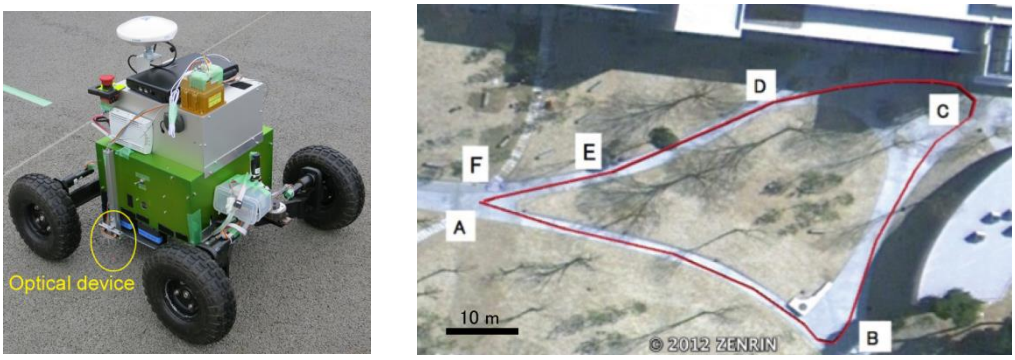

(a) Vehicle equipped with optical device (b) Course in campus of Tohoku University

Figure 22: Environment in campus for experiment.

4.2. Improving angle precision

The posture of a vehicle can be estimated by using two optical devices as discussed in the previous section. However, an error in angle accumulated because each optical device has an uncertainty in determining the translation. Estimating accurate posture in mobile robots is important because even a small error in posture results in a large positional error when the robot travels a long distance. To improve the accuracy of positioning a vehicle, we propose a combination of the modified optical device and a precise posture sensing system.

A sensing system using inertial sensors has been developed by our research group, and it provides the precise angle information of pitch φ and yaw θ. The inertial sensors consist of three 1-axis gyroscopes (Silicon Sensing CRS07-02S x2, CRS09-12 x1) and a 3-axis accelerometer (Crossbow CXL04GP3). The drift errors of the gyroscopes are automatically compensated for when no motion is detected in the system by the accelerometer. More details on drift error compensation of gyroscopes are provided by Nagatani et al. [19]. The vehicle position $(X,\ Y,\ Z)$ can be updated using φ and θ as in Eq. (8).

$$\begin{bmatrix} X^{f+1} \\ Y^{f+1} \\ Z^{f+1} \end{bmatrix} = \begin{bmatrix} v\cos\theta\cos\varphi \\ v\sin\theta\cos\varphi \\ v\sin\varphi \end{bmatrix} + \begin{bmatrix} X^{f} \\ Y^{f} \\ Z^{f} \end{bmatrix} \tag{8}$$

where *f* represents the frame number in a sequence of sensor data, and v is the translation estimated by an optical device in a frame time.

We developed a vehicle “El-Verde” with four driving wheels to examine the improved positioning method. For the original positioning method, two optical devices with bandpass filters and pipes were fixed at both sides of the vehicle, as shown in Figure 22(a). The distance between the optical devices

was 415 mm. For the improved positioning method, an optical device was attached under the body of the vehicle and used with inertial sensors. We compared the trajectories of both the original and improved positioning methods with ground-truth via an RTK-GPS (Trimble SPS852) equipped with a GPS antenna (Zephyr Model 2) in the vehicle. The RTK-GPS has a horizontal precision of 8 mm, a vertical precision of 15 mm, and a data rate of 20 Hz when it is used in a favorable conditions. The vehicle ran a paved course on the campus of Tohoku University, as shown in Figure 22(b). The marks "A" and "F" in the course indicate the start and goal point, respectively. The marks from "B" to "E" are break points for the purpose of drift error compensation, where the vehicle stopped for 3 s.

We conducted the experiment three times for the original positioning method and two times for the improved method. Figure 23 shows the trajectories of the positioning device and the ground-truth. The *X*-axis in the graph is fitted with the vehicle's orientation at the start point. The dashed line shows the trajectory of the RTK-GPS. The trajectories of the RTK-GPS partially deviated from the actual track at points near "C" and "D" because of multipath signals caused by a building. The solid line in Figure 23(a)-(c) is the trajectory of the original positioning method, and it incrementally digressed from the ground-truth because of the accumulated angle error. The solid line in Figure 23(d) and (e) from the improved positioning method is well-matched with the ground-truth.

The comparison of the conditions and results among all positioning methods in the experiment is shown in Table 1. The actual total run was estimated from the trajectory of the RTK-GPS in which we manually corrected the deviated portion of the path to be a smooth trajectory. All of the total runs estimated by the optical devices were smaller than that of the corrected RTK-GPS because of the tendency of optical devices to underestimate movement, as described previously with Figure 10. Each root mean square (RMS) error of position error in Figure 23 was calculated from the difference between the position measured by RTK-GPS and the estimated position by the device. Note that, in case that the RTK-GPS gave no reply, the RMS was not evaluated. The RMS errors from the improved method are below 1.7 m, which is much smaller than the errors from the original method, in spite of the long travel distance of over 190 m. This small error at the goal point from the improved method signifies that the gyroscopes contributed to precise posture measurements. The accuracy of the positioning using optical devices can be improved by using an accurate angle sensor for long distance traveling of mobile robots.

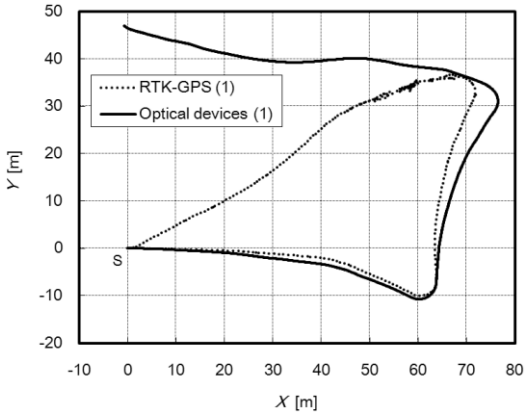

(a) Optical devices (1st)

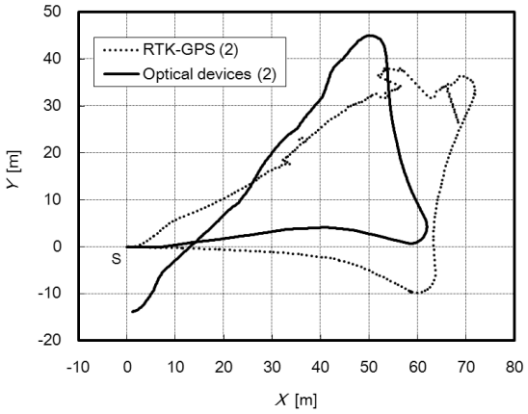

(b) Optical devices (2nd)

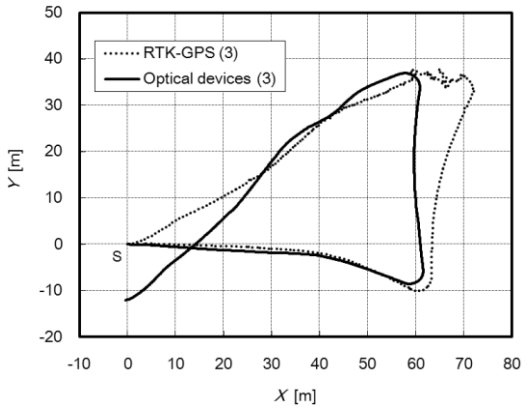

(c) Optical devices (3rd)

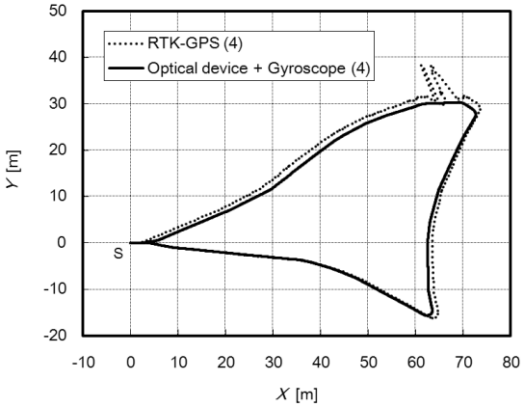

(d) Optical device and gyroscope (1st)

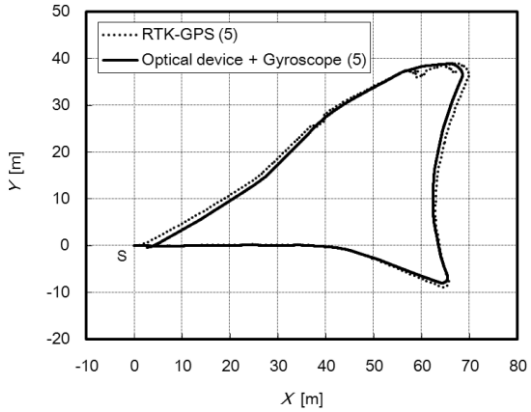

(e) Optical device and gyroscope (2nd)

Figure 23: Vehicle trajectories measured ("S" represents start point).

Table 1: Experimental conditions and measured results.

Condition		Result			
Sensor	Average velocity [m/s]	Total run			RMS error of trajectory [m]
		Corrected RTK-GPS [m]	Optical device [m]	Error [%]	
Optical devices (1st)	0.16	193.2	189.4	−1.97	17.6
Optical devices (2nd)	0.29	193.1	186.4	−3.46	11.0
Optical devices (3rd)	0.26	193.2	186.1	−3.65	7.4
Optical device and gyroscope (1st)	0.28	195.6	190.1	−2.77	1.7
Optical device and gyroscope (2nd)	0.25	196.5	192.4	−2.12	1.1

5. CONCLUSIONS

A positioning device using optical devices and laser light for outdoor mobile robots has been proposed. The optical device, designed for computer mice, is required to be used in contact with a surface. To extend the measureable distance between the device and the ground surface, a laser light source with collimated beams was employed. Two devices with laser sources were mounted to obtain the translation and rotation information of a mobile robot.

First, we evaluated the fundamental performance of the optical device through experiments. The external laser light had a consistent measurement error of translation within 1.6% at heights between 50 mm and 140 mm. This result indicates a region of height invariability of the device. The maximum measurable velocity of the device was investigated with an actuated turntable. The device tracked the motion of black paper at a velocity up to 1.8 m/s, which is sufficient for mobile robots. Through another experiment, we found that the shorter shutter period is imperative because the maximum velocity is dependent on the shutter period and the frame rate. The error of the device was between –1.6% and 0.2% for different surface materials.

Second, we proposed a method for restricting solar light using a bandpass filter and a pipe in order to use the positioning device in an outdoor environment. The device operated at an illuminance up to 70000 lx, whereas the functioning of the unmodified device stopped at 1600 lx. In an experiment where a vehicle equipped with the devices runs a course from an indoor start point to an outdoor goal point of 60000 lx, the estimated trajectories continued to the goal point in spite of errors in posture. The experimental result showed that the device that restricted solar light can be used in an outdoor environment.

Third, the errors of the estimated trajectory were significantly decreased by combining the optical device with gyroscopes; they offer more accurate angle information because the drift error is compensated for at break points. All the RMS errors of the trajectory from the improved method were

below 1.7 m in spite of a long travel distance of over 190 m.

As future work, we will extend the available area of the positioning device; we intend to use the device for positioning a mobile robot traversing rougher terrain.

Acknowledgments

This work was supported by MEXT/JSPS KAKENHI, Grant Number (21360110).

REFERENCES

[1] D. Maier and A. Kleiner, Improved GPS Sensor Model for Mobile Robots in Urban Terrain, in *Proc. of the IEEE Int. Conf. on Robotics and Automation*, Alaska, pp.4385-4390 (2010)

[2] J. D. Jackson, D. W. Callahan, and J. Marstrander, A Rationale for the use of Optical Mice Chips for Economic and Accurate Vehicle Tracking, in *Proc. of the IEEE Int. Conf. on Automation Science and Engineering*, Arizona, pp.939-944 (2007)

[3] F. M. Santos, V. F. Silva, and L. M. Almeida, A Robust Self-localization System for a Small Mobile Autonomous Robot, in *Proc. of the IEEE Int. Symposium on Robotics and Automation*, Mexico (2002)

[4] S. Lee and J. Song, Mobile Robot Localization Using Optical Flow Sensors, in *Int. Journal of Control, Automation, and Systems*, **2**(4), 485-493 (2004).

[5] J. A. Cooney, W. L. Xu, and G. Bright, Visual Dead-reckoning for Motion Control of a Mecanum-wheeled Mobile Robot, in *Mechatronics*, **14**(6), 623-637 (2004).

[6] A. Bonarini, M. Matteucci, M. Restelli, A Kinematic-independent Dead-reckoning Sensor for Indoor Mobile Robotics, in *Proc. of the Int. Conf. on Intelligent Robots and Systems*, Sendai, pp.3750-3755 (2004)

[7] D. Sekimori and F. Miyazaki, Precise Dead-reckoning for Mobile Robots Using Multiple Optical Mouse Sensors, in *Informatics in Control, Automation and Robotics II*, 145-151 (2007).

[8] J.-S. Hu, Y.-J. Chang, and Y.-L. Hsu, Calibration and On-line Data Selection of Multiple Optical Flow Sensors for Odometry Applications, in *Sensors and Actuators A* **149**(1), 74-80 (2009).

[9] M. Cimino and P. R. Pagilla, Location of Optical Mouse Sensors on Mobile Robots for Odometry, in *Proc. of the IEEE Int. Conf. on Robotics and Automation*, Alaska, pp.5429-5434 (2010)

[10] J. Palacin, I. Valganon, and R. Pernia, The Optical Mouse for Indoor Mobile Robot Odometry Measurement, in *Sensors and Actuators A* **126**, 141-147 (2006).

[11] W. Xin and K. Shida, Optical Mouse Sensor for Detecting Height Variation and Translation of a Surface, in *Proc of the IEEE Int. Conf. on Industrial Technology*, pp.1-6 (2008)

[12] M. Dille, B. P. Grocholsky, and S. Singh, Outdoor Downward-facing Optical Flow Odometry With Commodity Sensors, in *Proc. of Field & Service Robotics*, Massachusetts (2009)

[13] A. M. H. S. Abeykoon, L. Udawatta, M. S. Dunuweera, R. T. Gunasekara, M. Fonseka, and S. P. Gunasekara, Enhanced Position Sensing Device for Mobile Robot Applications Using an Optical Sensor, in *Proc of the IEEE Int. Conf. on Mechatronics*, Istanbul, pp.597-602 (2011)

[14] N. Tunwattanaa, A. P. Roskillya, and R. Normanb, Investigations Into the Effects of Illumination and Acceleration on Optical Mouse Sensors as Contact-free 2D Measurement Devices, in *Sensors and Actuators A* **149**(1), 87-92 (2009).

[15] I. Nagai, K. Watanabe, K. Nagatani, and K. Yoshida, Noncontact Position Estimation Device With Optical Sensor and Laser Sources for Mobile Robots Traversing Slippery Terrains, in *Proc. of the IEEE/RSJ Int. Conf. on Intelligent Robots and Systems*, Taipei, pp.3422-3427 (2010)

[16] R. Ross, J. Devlin, and S. Wang, Toward Refocused Optical Mouse Sensors for Outdoor Optical Flow Odometry, in *IEEE Sensors Journal*, **12**(6), 1925-1932 (2012).

[17] I. Yamaguchi, Theory and Applications of Speckle Displacement and Decorrelation, in *Speckle Metrology*, R. S. Sirohi, pp.1-39, Marcel Dekker, Inc., New York (1993)

[18] Avago Technologies, ADNS-6010 Laser Mouse Sensor Data Sheet, in *http://www.avagotech.com* (2008)

[19] K. Nagatani, N. Tokunaga, Y. Okada, and K. Yoshida, Continuous Acquisition of Three-Dimensional Environment Information for Tracked Vehicles on Uneven Terrain, in *Proc of the IEEE Int. Workshop on Safety, Security and Rescue Robotics*, pp.25-30, Sendai (2008)